Thin Solid Films, *201* (1991) 373–402
CONDENSED MATTER FILM BEHAVIOUR

ADSORPTION OF XENON ATOMS ON METAL SURFACES

S. ISHI
Tomakomai National College of Technology, Tomakomai 059-12 (Japan)
B. VISWANATHAN
Indian Institute of Technology, Madras 600036 (India)
(Received October 9, 1990; accepted January 8, 1991)

In recent times the adsorption of rare gases, especially xenon, on metal surfaces has been extensively used to rationalize certain basic features of the adsorption process. Available experimental data on the energetics of adsorption and other photoelectron spectroscopic measurements show that a chemical bonding model alone can explain adequately all the results reported in the literature. Detailed theoretical models have been developed to rationalize the features observed in photoelectron spectra.

1. INTRODUCTION

Adsorption studies constitute one of the ways of probing the nature and reactivity of clean metal surfaces. Of the various adsorption systems, rare gas adsorption on metal surfaces is particularly interesting and comparatively easy to study because of the weak nature of the interaction in these systems (see for example ref. 1). The ground state electronic configuration of inert gas atoms is a closed shell configuration. For example, helium has the configuration $(1s)^2$, while that of neon is $(1s)^2(2s)^2(2p)^6$. In the case of argon or any other inert gas atoms the electronic configuration of the ground state can be written as $\ldots(ns)^2(np)^6$ where n corresponds to the principal quantum number of the highest occupied shell. Since we are interested in the interaction of inert gas atoms with metal surfaces, it is necessary that we have some idea of the magnitude of the ionization energy of the highest occupied levels of the inert gases, as well as the magnitudes of the excitation energies. These data are assembled in Table I. The bonding interaction with metal surfaces might involve the highest occupied p states. This is deduced from a comparison of the magnitude of the difference between the ionization energy values of ns and np states, and for this purpose the ionization energies of ns states are also included in Table I.

It will be interesting to compare the reactivities of molecules which have similar ionization energies. The values of the ionization energies of the highest occupied states of argon, krypton and xenon are of similar magnitude to those of N_2 (15.60 eV), CO (14.01 eV) and O_2 (12.30 eV) respectively[5]. In spite of this, the

0040-6090/91/$3.50

TABLE I
IONIZATION[2,3] AND EXCITATION[4] ENERGIES FOR RARE GAS ATOMS

Gas	$np_{3/2}$	$np_{1/2}$	*ns*	$\lvert ns-np \rvert$	$(np)^6 \rightarrow (np)^5((n+1)s)^1$ *for the following values of J*			
					2	*1*	*0*	*1*
He			24.59					
Ne	21.56	21.66	48.42	26.8	16.62	16.67	16.71	16.85
Ar	15.76	15.94	26.30	13.5	11.55	11.62	11.72	11.83
Kr	14.00	14.67	27.40	13.2	9.91	10.03	10.56	10.64
Xe	12.13	13.44	23.39	10.8	8.31	8.43	9.45	9.57

J represents the total angular momentum in the excited states. All energies are in electronvolts. *n*p levels are virtual levels without spin–orbit (SO) interactions.

reactivities of these molecules with metal surfaces are quite different. The other relevant parameters which will be of interest with respect to the rare gas adsorption phenomenon are polarizability, atomic radius, the maximum number of rare gas atoms that can occupy a 1 m^2 area in a close-packed configuration, and the cohesive energy of solid rare gas systems. These data for the various rare gas atoms are given in Table II.

TABLE II
NUMERICAL VALUES OF THE POLARIZABILITY[6], ATOMIC RADIUS[6], H.C.P. MONOLAYER DENSITY AND F.C.C. COHESIVE ENERGY[6] FOR RARE GAS ATOMS

Gas	*Polarizability* ($\times 10^{-3}$ nm^3)	*Atomic radius* (nm)	*H.c.p. ML density* ($\times 10^{18}$ atoms m^{-2})	*F.c.c. cohesive energy* (kJ mol^{-1})
He	0.2	0.150	14.2	
Ne	0.4	0.159	12.6	1.88
Ar	1.6	0.191	7.9	7.74
Kr	2.5	0.201	7.2	11.18
Xe	4.0	0.220	6.0	14.94

ML, monolayer.

In the last 20 years, considerable emphasis has been placed on the study of photoemission and phase transition in two dimensions for rare gas atoms adsorbed on solid (metal) surfaces. The latter interest has arisen for a model of a quasi-two-dimensional (2D) system. Although it is conceived that rare gas adsorption on metal surfaces at low temperatures could be described in terms of the van der Waals interaction, the physicochemical consequences of rare gas adsorption do not seem to substantiate this concept. The purpose of this presentation is therefore to analyse the available experimental data for xenon gas adsorption on metal surfaces and to emphasize a chemical bonding model for treating rare gas–metal systems. The validity of this model will also be substantiated.

The present article is organized as follows. In the next section we present observations of the structure of the adsorbed xenon phase and the heat of adsorption. The experimental data on adsorption energies and work function

changes and their analysis in terms of charge transfer (CT) theory are dealt with in Section 3. In Section 4, the application of a variety of electron spectroscopies which provide information on the electronic structure of adsorbed xenon is considered.

2. STRUCTURE OF THE ADSORBED PHASE AND HEAT OF ADSORPTION

The adsorption of rare gases is used in practice to determine the surface area of powdered catalytic substances. In this estimation the rare gas atoms adsorbed in an ML are in an h.c.p. arrangement. The structure of adsorbed states has been examined by low energy electron diffraction, molecular beam diffraction, or high resolution helium scattering (HRHS), and neutron and X-ray diffraction. The structures of adsorbed xenon on various metal surfaces and the areas occupied by a xenon atom deduced from these measurements are given in Table III. At saturation coverage of the first ML, the structure of the adsorbed phase is almost h.c.p. and the area per atom at this coverage is 17×10^{-20} m^2.

TABLE III

ORDERED ADSORBED XENON PHASES AND AREA PER XENON ATOM ON VARIOUS METAL SURFACES

Substrate	*ML structure*	*Xe–Xe distance* (nm)	*Area per Xe atom* ($\times 10^{-2}$ nm^2)	*References*
Al(111)	H.c.p.	0.438	16.6	7
Cr(110)	centred (2 × 2)	0.494	21.2	8
Ni(100)	H.c.p.	0.452	17.8	9
Cu(111)	H.c.p.	0.442	16.9	10
Cu(100)	H.c.p.	0.450	17.5	11
Cu(110)	centred (2 × 2)	0.510	18.4	10, 12–15
	Compressed C(2 × 2)	0.460	16.6	10, 12–15
Cu(211)	H.c.p.	0.438	16.6	16
Cn(311)	H.c.p.	0.445	17.2	17
Pd(111)	$(\sqrt{3} \times \sqrt{3})$R30°	0.476	19.6	18
Pd(100)	H.c.p.	0.448	17.4	18, 19
Pd(110)	H.c.p.	0.449	17.5	18
Ag(111)	H.c.p.	0.450	17.5	20, 21
Ag(110)	Compressed C(2 × 2)	0.440	17.9	10
Ag(211)	H.c.p.	0.441	16.8	10
W(110)	(2 × 2)	0.894	28.3	22
	(7/10 × 2)[a]	0.632	20.2	22
	(7/10 × 4/7)[a]	0.553	17.6	22
Ir(111)	$(\sqrt{3} \times \sqrt{3})$R30°	0.480	19.9	23
	Incommensurate	0.440	16.6	23
Ir(100)1 × 1	H.c.p.	0.438	16.6	24
Ir(100)5 × 1	H.c.p.	0.438	16.6	24
Pt(111)	$(\sqrt{3} \times \sqrt{3})$R30°	0.480	19.9	23, 25, 26
	Incommensurate	0.435	16.4	23, 25, 26

[a] This structure is centred rectangular.

The evaluation of the structure of adsorbed phases is used for determining the phase transitions in 2D systems since in the case of rare gas adsorption the interaction with the substrate surface is at a minimum. For example, a phase

diagram of xenon adsorbed on Pt(111) is shown in Fig. 1[25], where at least six different phases have been observed so far and the coverage is defined with respect to the density of platinum atoms in the (111) substrate surface, *i.e.* $\theta_{Xe} = 1$ corresponds to 1.5×10^{19} Xe atoms m^{-2}. A xenon monolayer at low coverages ($\theta_{Xe} < 0.01$) has exhibited a 2D gas–solid phase transition, where the heat of evaporation of the 2D solid phase to the 2D gas phase is estimated as about 4.6 kJ mol^{-1} and at near-saturation coverages exhibits the following phases. For a coverage $\theta_{Xe} < 0.33$ and surface temperatures in the range $62\,K < T_s < 99\,K$ a $(\sqrt{3} \times \sqrt{3})R30°$ commensurate phase (C) exists, where T_s is the surface temperature. On completion of the commensurate phase at $\theta_{Xe} = 0.33$ or by cooling down the adlayer below 62 K the commensurate phase transforms in a continuous transition into a striped incommensurate phase (SI). In this striped phase, the xenon layer is uniaxially compressed along the ΓM_{Xe} direction, which is the notation for the surface Brillouin zone in the h.c.p. monolayer. On further increase in the adlayer density the striped phase (SI) transforms into a hexagonal incommensurate phase (HI) at coverages $\theta_{Xe} > 0.38$. The HI phase displays a continuous transition from an R30° to a rotated $R30° \pm 3.3°$ orientation (HIR) on further coverage increase ($\theta_{Xe} > 0.39$). This is the first system exhibiting completely the sequence C → SI → HI → HIR predicted theoretically by Bak *et al.*[27]

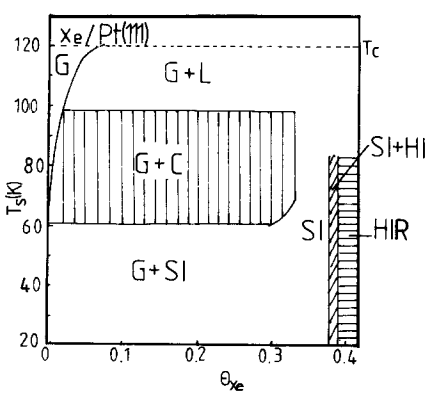

Fig. 1. Schematic phase diagram of xenon monolayers on Pt(111)[25]:G and L denote the 2D gas and the 2D liquid respectively; C, SI, HI and HIR phases are referred to in the text; T_c is the critical temperature.

Xenon adsorption on Cu(110) has also been investigated in detail to probe the commensurate–incommensurate phase transitions[28]. However, these studies have not yet reached a stage where unambiguous interpretation is possible, as more than one incommensurate structure for adsorbed xenon on Cu(110) is already known to exist. Further, the variety of structures of the adsorbed state as shown above can increase the utility of this system for the study of phase transitions in two-dimensional systems.

The isosteric heat of adsorption can be determined from the adsorption isotherms or isobars, which are measured using Auger electron spectroscopy (AES)[29], UV photoelectron spectroscopy (UPS)[30,31] or HRHS[25] for the evaluation of surface coverage. Measurements of the heat of adsorption as a function of

coverage provide information on the variation in binding energy with adatom concentration and thus reflect the influence of lateral interaction energies which are attractive or repulsive. Similar quantities are obtained by thermal desorption spectroscopy[32] with varying initial coverages.

Coverage dependence of the heat of adsorption of xenon adsorbed on various metal surfaces is shown in Fig. 2, where the trend of variation for Pd(100)[18,31], Ni(100)[9] and Cu(110)[13,15] appears to be different from that for Pt(111)[25], although the data are limited because of the difficulty of measurement. In the former case, a continuous decrease has been recorded until monolayer coverage while in the latter the trend is the opposite: the initial heat of adsorption at $\theta < 0.025 (\theta_{Xe} < 0.01)$ is 26.8 kJ mol^{-1} (277 meV) and it increases steadily to about 30.1 kJ mol^{-1} (312 meV) at $\theta = 0.83$ ($\theta_{Xe} = 0.33$). At coverages $\theta > 0.83$, a drop in the value of the heat of adsorption to 27.2 kJ mol^{-1} (281 meV) is observed. Here we use the coverage which is defined in terms of the density of adatoms in the monolayer, *i.e.* $\theta = 1$ corresponds to a saturation coverage with $N = 6 \times 10^{18}$ Xe atoms m^{-2}. Thus the continuous decrease or increase in the heat of adsorption with increasing coverage is indicative of repulsive or attractive mutual interactions respectively. This suggests that the origin of these interactions is mainly quantum mechanical, among the electrons and/or with electrons through metals, and that they are not electrostatic interactions such as dipole–dipole interactions, since the sign of the work function change due to xenon adsorption on metal surfaces is the same for all these metals as will be described in the next section, *i.e.* the polarity of xenon adatoms for these systems is always positive.

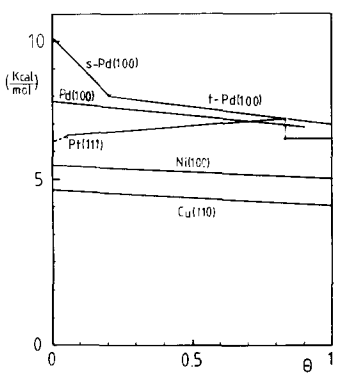

Fig. 2. Variation in the heat of adsorption with coverage for xenon on various metal surfaces: stepped (s-) and terrace (t-) Pd(100)[31]; Pd(100)[19]; Pt(111)[25]; Ni(100)[9]; Cu(110)[12].

3. ADSORPTION ENERGY AND WORK FUNCTION CHANGE FOR XENON ADSORPTION ON METAL SURFACES

Mignolet was the first to observe that the work function of the metals is decreased as a result of xenon adsorption[33]. He considered this decrease in work function to be due to an induced polarization effect. However, subsequently, he accounted for the work function decrease in terms of Mulliken's CT[34–36] (see also ref.

37) model as described below. Generally the interaction of rare gases with metal surfaces is thought to be due to van der Waals' forces[35]. This is reflected in the value of the adsorption energy. For example, for helium adsorption on metal surfaces, the adsorption energy is the least, 0.84 kJ mol^{-1}. However, in the case of xenon adsorption on transition metal surfaces, the interaction energy is of the order of 16–50 kJ mol^{-1} while for simple metal surfaces its magnitude is almost equal to or less than the cohesive energy of solid xenon. It is therefore clear that for xenon adsorption both the van der Waals force and CT interactions are involved in bonding[38–46].

Suhrmann *et al.*[47] have determined the work function changes by a photoemission method for xenon adsorption on evaporated nickel films. They observed a work function decrease of 0.7–0.9 eV. They have also observed that the electrical conductivity of the metal film increases with xenon adsorption. Ehrlich and Hudda[48], Gomer[49], Rootsaert *et al.*[50] and Ichizuka[51] have also observed work function changes of a similar magnitude on xenon adsorption by field emission microscopy (FEM). The authors of refs. 48–50 considered the adsorption of xenon on tungsten (polycrystalline) and reported a work function change of the order of 1.4 eV. Ichizuka studied xenon adsorption on rhenium surfaces and reported a value of 1.1 eV for the work function change. Engel and Gomer[39] as well as Nieuwenhuys *et al.*[52,53] have studied the work function changes as a result of xenon adsorption on single-crystal surfaces by the probe–hole technique. Engel and Gomer studied xenon adsorption on tungsten surfaces while Nieuwenhuys *et al.* considered xenon adsorption on iridium[52] and platinum[53] surfaces. The measurements on single crystals can also be made by photoelectron spectroscopy (PES)[9,18,54,55].

In Table IV the values of initial adsorption energies and work function changes observed at saturation coverage are summarized. From these data one can generate a relationship between adsorption energy E and work function $\Delta\phi$ as shown in Fig. 3, where circles and triangles represent data for single crystals and polycrystalline metal surfaces respectively. The first paper in which a plot of E *vs.* $\Delta\phi$ on different

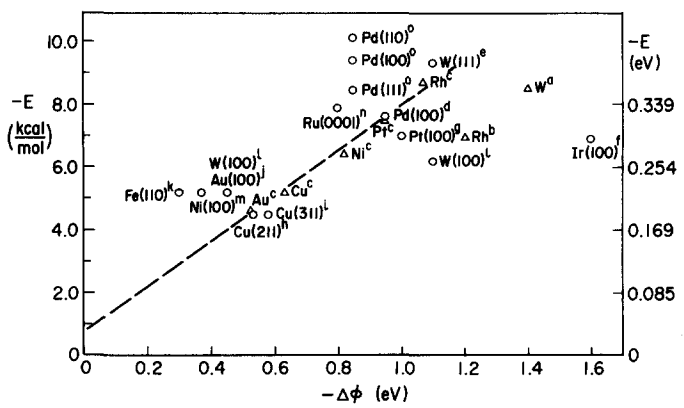

Fig. 3. Relationship between adsorption energy and work function change on metal surfaces from the following references: a, 48, 49; b, 71; c, 40; d, 19; e, 79; f, 52; g, 43; h, 16; i, 17; j, 80; k, 55; l, 43; m, 9; n, 68; o, 18.

TABLE IV

OBSERVED WORK FUNCTION CHANGES $\Delta\phi$ AT SATURATION COVERAGE AND INITIAL ADSORPTION ENERGIES E FOR XENON ON VARIOUS METAL SURFACES[a]

Substrate	$\Delta\phi$ (eV)	E (kJ mol^{-1})	*References*
Li(poly)	0.1 (CP)		56
Na(poly)	0.05 (CP)		56
Na(poly)	≈0.0 (RP)		57
Mg(poly)	0.3 (CO)		56
Al(111)	0.3 (PES)	51.9 (D)	58
Al(poly)	0.25 (CP)		56
K(poly)	≈0.0 (CP)		34
K(poly)	0.05 (CP)		56
Ca(poly)	≈0.0 (CP)		34
Ti(poly)	0.84 (CP)		34
Ti(poly)	0.70 (CP)		59
Cr(poly)	0.95 (CP)		34
Fe(110)	0.3 (PES)	21.8 (ISO)	55
Fe (poly)	0.36 (PE)	28.9 (ISO)	60
Fe (poly)	0.66 (CP)		34
Ni(111)		20.9	61
Ni(100)	0.38 (CP, PES)	21.8 (ISO)	9
Ni(100)	0.40 (PES)		62
Ni(110)	0.75 (PES)		63
Ni(poly)	0.82 (PE)	26.8 (ISO)	40
Ni(poly)	0.36 (PE)	23.9 (ISO)	60
Ni(poly)	0.85 (CP)		34
Cu(111)	0.48 (CP)		10
Cu(100)	0.47 (CP)		10
Cu(100)		26.0 (ISO)	29
Cu(110)	0.61 (CP, PES)		10, 64
Cu(110)		19.3 (ISO)	10
Cu(211)	0.53 (CP)		16
Cu(311)	0.58 (CP)	18.8 (ISO)	17
Cu(610)		27.2 (ISO)	65
Cu(poly)	0.63 (PE)	21.8 (ISO)	40
Cu(poly)	0.57 (RP)		57
Zn(poly)	0.21 (CP)		34
Se(poly)	0.1 (CP)		34
Zr(poly)	0.65 (CP)		66, quoted in ref. 57
Mo(poly)	1.4 (FEM)		67
Mo(poly)	0.95 (CP)		59
Ru(0001)		25.1 (ISO)	68
Ru(0001)	0.65 (PES)		69
sk-Ru(0001)[b]		35.6 (D)	68
Ru(poly)	0.95 (FEM)		70
Rh(poly)	1.08 (PE)	36.4 (ISO)	40
Rh(poly)	1.20 (FEM)	29.3 (D)	71
Pd(111)	0.85 (PES)	34.8 (D)	18
Pd(100)	0.94 (PES)	40.6 (D)	18
Pd(100)	0.65 (PES)		72
Pd(110)	0.92 (PES)	42.7 (D)	18
Pd(poly)	0.55 (PE)	22.2 (D)	60
Pd(poly)	1.12 (FEM)		70
Ag(111)	0.44 (CP)		10
Ag(111)		18.0 (ISO)	20
Ag(111)		21.8 (D)	73

TABLE IV–*continued*

Substrate	$\Delta\phi$ (eV)	E (kJ mol^{-1})	*References*
Ag(111)	0.47 (PES)	21.8 (D)	21
Ag(110)	0.45 (CP)		10
Ag(110)		25.5 (ISO)	74
Ag(211)	0.45 (CP)		10
Ag(poly)	0.47 (RP)		75
Ag(poly)	0.18 (PE)	21.8 (ISO)	60
Sn(poly)	≈0.0 (RP)		57
Cs(poly)	≈0.0 (RP)		57
Cs(poly)	0.025 (CP)		56
Ta(110)	1.0 (PES)		76
W(110)	2.4 (FEM)	38.5 (D)	39
W(110)	0.45 (CP)	22.2 (D)	77
W(110)	1.50 (FEM)		78
W(100)	1.35 (FEM)	24.7 (D)	39
W(100)	1.10 (CP)	26.0 (D)	77
W(100)	0.9 (FEM)		78
W(111)	1.13 (FEM)	24.7 (D)	39
W(111)	1.1 (RP)	38.9 (D)	79
W(111)	0.6 (FEM)		78
W(210)	1.4 (FEM)	26.8 (D)	39
W(211)	0.92 (FEM)	27.2 (D)	39
W(211)	1.0 (FEM)		78
W(poly)	1.4 (FEM)	35.6 (D)	48
W(poly)	1.14 (CP)		34
Re(poly)	1.1 (FEM)		51
Ir(111)	1.8 (FEM)	29.3 (D)	52
Ir(100)[c]	1.6 (FEM)	28.9 (D)	52
Ir(110)[c]	0.8 (FEM)	27.2 (D)	52
Ir(210)[c]	1.3 (FEM)	29.3 (D)	52
Ir(321)[c]	1.0 (FEM)	31.8 (D)	52
Ir(poly)	1.18 (FEM)		52
Ir(poly)	1.05 (FEM)		70
Pt(111)	0.6 (PES)		23
Pt(111)		29.3 (D)	53
Pt(100)	1.0 (FEM)	29.3 (D)	53
Pt(110)[c]		28.5 (D)	53
Pt(110)(2 × 1)		33.5 (D)	80
Pt(210)[c]	1.1 (FEM)	29.3 (D)	79
Pt(321)[c]	0.9 (FEM)	31.0 (D)	53
Pt(311)[c]	0.9 (FEM)		53
Pt(poly)	0.95 (PE)	31.8 (ISO)	40
Pt(poly)	0.68 (PE)	28.9 (ISO)	60
Au(100)	0.45 (CP)	21.8 (ISO)	81
Au(poly)	0.52 (PE)	19.3 (ISO)	40
Au(poly)	0.50 (RP)		82
Hg	0.23 (CP)		34
Gd	0.6 (PES)		83

[a] The techniques used for the measurements of $\Delta\phi$ and E are given in parentheses: CP, measurement of contact potential difference; RP, measurement of retarding potential difference; PE, photoelectric emission; D, measurement of desorption; ISO, isothermal or isosteric measurement; other abbreviations are defined in the text.

[b] sk, stepped–kinked surfaces.

[c] Includes the influence around the faces.

metals was reported is ref. 40. It is seen that a linear relationship, shown by the broken line, exists between these two parameters[45,46]. This relationship can be rationalized as follows[1].

The total approximate wavefunction of the system can be written

$$\Psi_t = a\varphi(\mathrm{MXe}) + b\varphi(\mathrm{M^-Xe^+}) \tag{1}$$

where $\varphi(\mathrm{MXe})$ is the wavefunction for neutral xenon adsorbed on metal surfaces and $\varphi(\mathrm{M^-Xe^+})$ is the wavefunction after transfer of a 5p electron of xenon to the metal. The symbols for the coefficients of the wavefunctions and matrix elements in the present section are written as real for simplicity of notation. Assuming that the overlap integral is small and therefore can be neglected, one can write the normalization condition as

$$a^2 + b^2 = 1 \tag{2}$$

The energy W_a of the ground state of the adsorption system is given by

$$W_a = \langle \Psi_t | H | \Psi_t \rangle \approx W_0 - \frac{V^2}{W_1 - W_0} \tag{3}$$

where H is the total hamiltonian and W_0, W_1 and V are defined as

$$W_0 = \langle \varphi(\mathrm{MXe}) \,|\, H \,|\, \varphi(\mathrm{MXe}) \rangle \tag{4a}$$

$$W_1 = \langle \varphi(\mathrm{M^-Xe^+}) \,|\, H \,|\, \varphi(\mathrm{M^-Xe^+}) \rangle \tag{4b}$$

$$V = \langle \varphi(\mathrm{M^-Xe^+}) \,|\, H \,|\, \varphi(\mathrm{MXe}) \rangle \tag{4c}$$

In this formulation, the condition $V \ll W_1 - W_0$ has been assumed. W_0 represents the total energy of separated metal and xenon atom in their ground states. Therefore the adsorption energy E is given by

$$E = W_0 - W_a = \frac{V^2}{W_1 - W_0} \tag{5}$$

The value of the ratio of the coefficients in the wavefunction is given by

$$\frac{b}{a} = \frac{V}{W_1 - W_0} \tag{6}$$

where $a^2 \approx 1$; then

$$b^2 = \left(\frac{V}{W_1 - W_0} \right)^2 \tag{7}$$

The Helmholtz equation for the work function change[1,39] is given by

$$\Delta\phi = 4\pi\mu N_A = 4\pi\mu N\theta, \qquad \mu = eb^2 D \tag{8}$$

where μ is the dipole moment per adsorbed xenon atom, $N_A = N\theta$ corresponds to the number of atoms adsorbed per unit area, e is the elementary electric charge and D is the distance between the metal surface and adsorbed xenon atom. Since $\Delta\phi$ is related to b^2, then, with the help of eqns. (5)–(8), the expression for the relationship

between E and $\Delta\phi$ is given as

$$E = (W_1 - W_0)b^2 = \frac{W_1 - W_0}{4\pi NeD}\frac{\Delta\phi}{\theta} \tag{9}$$

Equation (9) shows that E is proportional to $\Delta\phi$.

One can estimate the value of the coefficient in eqn. (9). $W_1 - W_0 = I - \phi - e^2/4D$ (ref. 39) = 6 eV where I is the ionization energy of a xenon atom, ϕ is the work function of the metal (4.5 eV) and $e^2/4D$ is the value of the image potential (1.6 eV) when the value of D is assumed to be 0.22 nm. Since the work function changes observed are of the order of 1 eV at $\theta = 1$, the interaction energy E should be of the order of 24 kJ mol^{-1} (0.25 eV). The effective charge as deduced by this model is about $0.04e$, so that the value of the dipole moment is 0.5 debye, where the adsorbed number N of adatoms is assumed to be 6×10^{18} m^{-2}. If, in addition, one were to assume that the interaction energy due to van der Waals' forces is of the same order, then the interaction energy will have a magnitude of about 50 kJ mol^{-1}, which is about twice the experimental values reported in Table IV. However, qualitatively the CT model could account for the magnitude of both of the experimental parameters. It should be remembered that we have considered only the attractive terms in this model. A realistic model should also take into account the repulsive interactions[42,44], if one were trying to obtain the correct magnitudes of the values of the interaction energy. Although such a theoretical calculation can be made by the density functional approach[44], these calculations have not yet been successful.

One can compare the values of changes in work function as well as adsorption energies of krypton with those of argon. However, this comparison is limited owing

TABLE V

OBSERVED WORK FUNCTION CHANGES $\Delta\phi$ AT SATURATION COVERAGE AND INITIAL ADSORPTION ENERGIES E FOR KRYPTON AND ARGON ON VARIOUS METAL SURFACES[a]

Substrate	*Kr*		*Ar*		*Reference*
	$\Delta\phi$ (eV)	E (kJ mol^{-1})	$\Delta\phi$ (eV)	E (kJ mol^{-1})	
Al(111)	0.187 (PES)		0.143 (PES)		84
Fe(poly)		17.6 (ISO)			60
Ni(100)	0.25 (CP)		0.165 (CP)		9
Ni(poly)		18.0 (ISO)			60
Cu(111)		14.7 (ISO)			85
Cu(110)	0.29 (PES)		0.19 (PES)		86
Cu(110)		12.6 (ISO)			13
Cu(211)	0.35 (CP)				16
Cu(poly)		15.1 (ISO)			38
Pd(100)	0.36 (PES)	19.3 (ISO)			87
Pd (poly)	0.24 (PE)	21.8 (ISO)			60
Ag(111)	0.29 (CP)				16
Ag(111)		14.7 (ISO)		9.6 (ISO)	73
Ag(poly)		20.9 (ISO)			60
Pt(poly)	0.32 (PE)	23.9 (ISO)			60
Pt(poly)		14.7 (ISO)		9.6 (ISO)	88

[a] The techniques used for the measurements of $\Delta\phi$ and E are given in parentheses: see Table IV.

to restrictions in krypton or argon adsorption, which requires very low temperatures. The limited data available are summarized in Table V. It is seen that even in these systems the work function change is the same order of magnitude as that for xenon adsorption on metals, although the absolute magnitudes are smaller than that for xenon adsorption on metals. If one were to assume that the same model is applicable for krypton and argon adsorption, then one can reconcile these lower magnitudes since the ionization energies of the 3p and 4p levels of argon and krypton are higher than that of the 5p level of xenon.

4. ELECTRONIC STRUCTURE OF ADSORBED XENON

4.1. Introduction

There are a variety of experimental tools available for the study of adsorption phenomena. Among these, electron spectroscopy[89–92] has a prominent place in the determination of the amount and the structure of adsorbates as well as the nature of adsorption. It is known that the study of the electronic structure of adsorbates is important in understanding the bonding scheme in the adsorbed phase. PES is capable of providing information on the electronic structure of adsorption systems. Since 1970, PES has been extensively used for the study of the chemisorption of various species on metal surfaces[89]. However, the analysis of spectra of such systems is complicated because of the variations in the interaction between the adsorbate and the metals. It is normally expected that the analysis of the spectra of rare gas atoms adsorbed on metals is simpler because of the weak interaction between the adsorbate and the metal surfaces.

PES[89,90] notably provides information on the occupied levels of the species probed while unoccupied levels can be probed using bremsstrahlung isochromatic spectroscopy or inverse PES (IPES)[91,92]. Electron energy loss spectroscopy (EELS)[93] provides information on the excited states of the species probed. It is therefore necessary to combine all three of these techniques to understand the totality of the electronic structures of adsorbed systems.

A schematic representation of the processes taking place in each of these three techniques and the corresponding energy conservation equations is given in the following:

Technique	*Process and energy equation*
PES	$h\nu + A \rightarrow A^+ + e^-$; $h\nu^{in} - E^{out} = \varepsilon$ (occupied levels)
IPES	$e^- + A \rightarrow A^- + h\nu$; $E^{in} - h\nu^{out} = \varepsilon$ (unoccupied levels)
EELS	$e^- + A \rightarrow A^* + e^-$; $E^{in} - E^{out} = \varepsilon$ (excited levels)

Here $h\nu^{in}$ and $h\nu^{out}$ represent the photon incident and outgoing, E^{in} and E^{out} represent the electron energy incident or ejected, A represents the neutral atom or species and $A^i, i = +, -, *$, represent positive ion, negative ion and excited states; in other words, the neutral atom or species A is shown for the initial state, while A^+, A^- and A^* represent the final states observed in each of these techniques.

4.1.1. Presentation of available data

In the UPS spectra of xenon atoms adsorbed on metal substrate two peaks are

observed in the region 5–8 eV with respect to the Fermi level which are designated as μ_1 and μ_2 as shown in Fig. 4[94]. The shapes of these peaks are dependent on the nature of the metal as well as the coverage. The study of the adsorbed states of xenon on metal surfaces with UPS is called photoemission of adsorbed xenon (see for example ref. 95), or rare gas titration[96], which has gained importance in recent times as a powerful technique for surface analysis on atomic dimensions.

Waclawski and Herbst have reported the first observations by UPS of adsorbed xenon on W(100)[97]. The spectra observed are similar to those of the gas phase. That is, two peaks are observed which are due to SO interactions and are assigned as due to $^2P_{3/2}$ and $^2P_{1/2}$ levels respectively. The separation between these two peaks is 1.3 eV[4]. In addition, the shape of the μ_1 peak is broadened more than is that of the μ_2 peak with respect to those observed for gas phase xenon. In Fig. 4 the UPS spectra of xenon on W(110) are shown for various coverages. It can be seen that the peak is broadened as a function of coverage and in particular the splitting peak is seen even at a low coverage $\theta = 0.14$.

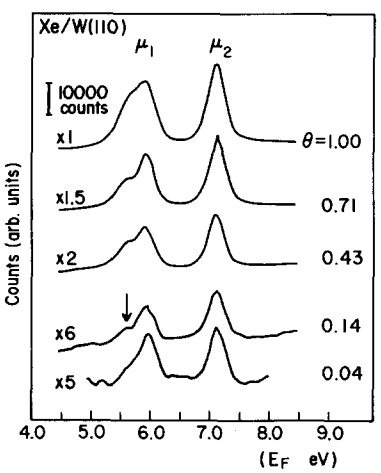

Fig. 4. UPS spectra as a function of coverage for Xe–W(110)[92].

Waclawski and Herbst attempted to interpret this broadening on the basis of crystal field theory. According to this postulate, the charge on the metal atoms has to be 0.5*e*, which is unrealistically high[98]. In addition, the angle-resolved UPS spectra[99] observed cannot be explained on the base of crystal field theory. Instead of using crystal field theory, Matthew and Devey[100], and independently Antoniewiez[98], explained the results in terms of an image charge screening model. According to this model, as the xenon atom approaches the metal surface the $^2P_{3/2}$ state is split into two states such as $^2P_{3/2}(m_J = \pm 3/2$ or $m_J = \pm 1/2)$. The charge distributions of these two states $^2p_{3/2}(m_J = \pm 3/2$ or $m_J = \pm 1/2)$ are different and the image potentials are also different, with the result that the order of splitting in $^2P_{3/2}(m_J = \pm 3/2)$ is higher than that in $^2P_{3/2}(m_J = \pm 1/2)$. Horn *et al.*[101] reported UPS spectra of xenon adsorbed on Pd(100) as a function of coverage. In these spectra the broadening is remarkable at coverages greater than 0.7. They considered that at

high coverages the lateral interaction between the adsorbed xenon atoms might cause the degenerate $^2P_{3/2}$ level to split into two states, where the order of split levels is $^2P_{3/2}(m_J = \pm 3/2) < {}^2P_{3/2}(m_J = \pm 1/2)$. This ordering, which is also derived on the basis of theoretical calculations in a two-dimensional band dispersion model [102,103], is the opposite to that proposed by image charge theory.

The splitting in levels is considered to be due to some perturbations as described above. However, these theories have not explicitly considered the effect of the adsorption phenomenon itself[104]. If one were to consider this bonding effect also, then the 5p orbitals of the xenon atom will be split into 5pσ and 5pπ orbitals for the case of interaction of the xenon with metal surfaces. The resultant ordering of the split energy levels is the same as that obtained with the image potential model. Since the integrated experimental spectra are inadequate for deciding the ordering of energy levels, the spin-resolved photoelectron spectra (SRPES) by Schönhense[23] are powerful for doing it.

Schönhense[23] also reported the excitation spectra with SRPES for xenon adsorbed on graphite, an example of which is shown in Fig. 5(b), together with similar excitation spectra as a function of exposure obtained with EELS for the Xe–Au adsorption system[93].

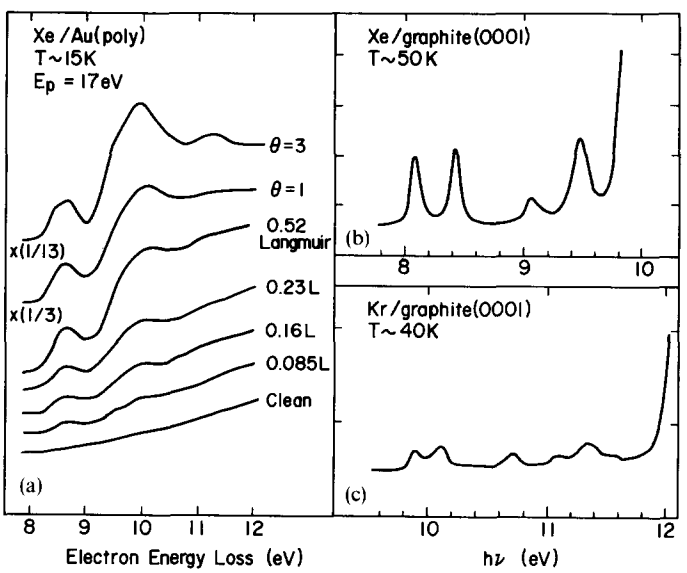

Fig. 5. Excitation spectra for (a) Xe–Au, and (b) xenon and (c) krypton adsorbed on graphite(0001), obtained by EELS[93] and SRPES[23].

Valence–core level binding energy or ionization energy shifts during adsorption have been considered[90]. The binding energy or ionization energy shift ΔI, which is defined as $\Delta I = \Delta I^{v}_{gas} - I^{v}_{ads}$ where I^{v} is the ionization energy with respect to the vacuum level, is rationalized in terms of an "initial state" effect ΔI_i (an environment effect caused by the initial chemical interaction) or a "final state" effect ΔI_f arising

from the relaxation process taking place in the system after the ejection of the outgoing particle.

The values of ΔI for a wide variety of substrates are summarized in Table VI, where the substrates are grouped in accordance with their different surfaces: (A) is the bare metal surface ((A_0) when $\theta \to 0$, (A_1) when $\theta \to 1$); (B) is the second xenon layer; (C) is the first layer of species such as CO, C_2H_2, atomic oxygen and atomic carbon on metal surfaces; (D) is the third xenon layer (D_1), the xenon multilayer beyond the third layer (D_2) or the multilayer of molecular species (H_2O, N_2, CO) (D_3). From Table VI, it is seen that the magnitude of ΔI is of the order of 1–2 eV irrespective of the nature of the metal surface. Interpretations of this shift have been presented by several workers. In an early publication, Wandelt[95] took ΔI to be the sum of the initial effect and the final effect and then explained ΔI as due to the work function decrease on xenon adsorption; in other words[109], "the Xe levels are pinned

TABLE VI
ENERGIES FOR XENON PHOTOELECTRON SPECTROSCOPY SHIFTS

Substrate	ΔI (eV)	$-\Delta E$ (eV)	$-\Delta E^+$ (eV)	I_{ads} (eV)	I^F (eV)	ϕ (eV)	$-\Delta\phi$ (eV)	*Reference*
(A_0):1 ML,$\theta \to 0$								
Ni(100)	1.27	0.24	1.51	12.13	6.83	5.30		9
Ni(110)	1.25	0.24	1.49	12.15	7.60	4.55		63
Ru(0001)	1.12	0.25	1.37	12.28	6.76	5.52		69
Pd(111)	0.98	0.36	1.34	12.42	6.47	5.95		18
Pd(100)	1.00	0.41	1.41	12.40	6.75	5.65		18
Pd(110)	1.17	0.44	1.26	12.23	7.03	5.20		18
Ag(111)	1.02	0.23	1.26	12.38	7.62	4.76		21
W(100)	0.90			12.50				99
W(110)	1.17	0.19	1.36	12.23	7.13	5.10		94
Pt(111)	1.10	0.31	1.41	12.30	5.90	6.40		105
Al(111)	1.18			12.22	7.74	4.48		69
Al(111)	1.11			12.29				7
(A_1):1 ML,$\theta \to 1$								
Ni(100)	1.65	0.23	1.88	11.75			0.38	9
Ni(110)	2.00	0.23	2.23	11.40			0.75	63
Ru(0001)	1.77	0.17	1.94	11.63			0.65	69
Pd(111)	1.55	0.35	1.90	11.85	6.75		0.85	18
Pd(100)	1.66	0.39	2.05	11.74	6.95		0.86	18
Pd(100)	1.71	0.39	2.10	11.69			0.65	106
Pd(110)	1.75	0.40	2.15	11.65	7.35		0.90	18
Ag(111)	1.49	0.25	1.74	11.91			0.47	21
W(100)	1.90			11.50			(1.00)	99
W(110)	1.52	0.19	1.71	11.88			0.35	94
Ir(111)	2.28			11.12				23
Pt(111)	2.26			11.14			0.60	23
Al(111)	1.80			11.60			0.29	7
Cs(poly)	1.10	0.13	1.23	12.30			≈ 0	107
Graphite	1.89	0.24	2.13	11.51			−0.10	23
ZnO	1.10	0.17	1.27	12.30			≈ 0	108

TABLE IV–*continued*

Substrate	ΔI (eV)	$-\Delta E$ (eV)	$-\Delta E^+$ (eV)	I_{ads} (eV)	I^F (eV)	ϕ (eV)	$-\Delta\phi$ (eV)	*Reference*
(B): 2 ML								
Ni(110)	1.30			12.10	8.30		0.75	63
Ru(0001)	1.18			12.22	7.35		0.65	69
Pd(111)	0.83			12.57	7.47		0.85	69
Pd(100)	1.01	0.22	1.23	12.39	7.60		0.86	69
Pd(100)	1.10			12.30			0.65	106
Ag(111)	0.96	0.17	1.13	12.44	8.15		0.47	21
W(110)	0.99	0.14	1.13	12.41	7.66		0.35	94
Pt(111)	1.63	0.21	1.84	11.77			0.60	23
Al(111)	1.30			12.10				69
Al(111)	1.01			12.39	8.20		0.29	7
Graphite	1.18	0.21	1.39	12.22				23
(C)								
CO/Ni(110)	0.80			12.50	6.30		−1.65	63
CO/W(110)	1.89			11.51	5.86		−0.55	94
α-C_2H_2/Pd(100)	1.27			12.13	7.28		0.80	69
β-C_2H_2/Pd(100)*	1.20			12.20	6.95		0.40	69
C_2H_2/Pd(100)*	1.21			12.19	7.74		1.20	69
C_6H_6/Pd(100)*	1.23			12.17	7.92		1.40	69
O/Pd(100)	0.95			12.35	6.60		−0.55	69
O/W(110)	1.14			12.26	6.26		−0.90	94
C/Pt(111)	1.91			11.49				23
(D_1): 3 ML								
Ni(110)	1.20			12.20	8.50		0.85	63
Pd(100)	1.04	0.19	1.23	12.36	7.80		1.09	69
Ag(111)	0.86	0.15	1.01	12.54	8.33		0.55	21
Al(111)	1.10			12.30				7
Cs(poly)	1.10			12.30				107
(D_2): multilayer								
Pd(100)	0.90			12.50				106
Cs(poly)	1.10			12.30				107
ZnO	1.10			12.30				108
(D_3)								
N_2/H_2O/Ni(110)	1.15			12.55	8.80		1.10	54
N_2/N_2/Ni(110)	0.85			12.55	8.05		0.05	54
N_2/CO/Ni(110)	0.85			12.55	6.35		−1.65	54
Xe(gas)				13.40				

ΔI, shift (see eqn. (10), Section 4.2); ΔE, ΔE^+, interaction energies of the ground and ionic states respectively; I_{ads}, I^F, ionization energies with respect to vacuum and Fermi levels respectively; θ, $\Delta\theta$, work function for clean metal surface and work function change for which a coverage $\theta_{Xe} = 1$ is supposed for the monolayer range respectively; values in parantheses are estimates;* thick, condensed interlayer (see ref. 69).

to the vacuum level". At the same time, Jacobi *et al.*[54,63,107] reported UPS spectra of the various molecules adsorbed on clean metal surfaces as well as those of xenon on

multilayers of other gaseous molecules. They concluded that the magnitude of ΔI due to the image potential effect is smaller than that observed for the xenon–metal system and therefore the cause of binding energy shift in the latter system should be due to an initial state effect. On the contrary, Kaindl and others[110] have reported the core and Auger spectra of adsorbed xenon on metal substrates as a function of adsorbed layer and ascribed the layer-dependent shifts to the final state effect or the final relaxation effect.

More recently, Jacobi and Astaldi[113,114] re-examined the relation between the binding energy shift and the change in work function due to adsorption and disagreed with the earlier view of Jacobi *et al.*[54,63,107]

In recent times, since the utility of IPES has been demonstrated, it has rapidly become an essential technique for the study of the electronic structure of solids and solid surfaces. There has been a similar controversy in the binding energy shifts for xenon–metal adsorption systems observed by IPES[115,116]. In Fig. 6, two sets of spectra are given. One set has been reported by Horn *et al.*[115], while the other is from Wandelt *et al.*[116] It is seen that in one case the binding energies of the peaks shift to higher values as a function of the number of layers while in the other case the opposite trend is observed. One of the assignments has to be wrong.

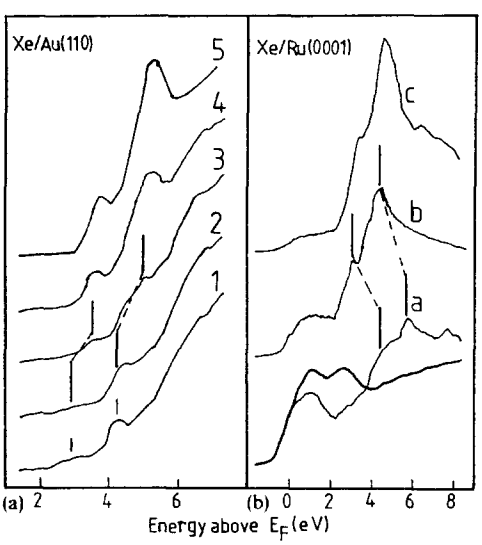

Fig. 6. IPES spectra as a function of coverage for (a) Xe–Au(110)[115] (spectra of adsorbed xenon at ML coverage (curve 1), of the incomplete bilayer (curve 2), of the complete bilayer (curve 3), of three layers (curve 4) and for five layers (curve 5)) and (b) Xe–Ru(0001)[116] (spectra of the clean surface (——) and surfaces with 18 langmuirs (curve a), 40 langmuirs (curve b) and 100 langmuirs (curve c)).

In the following, we consider the cause of the binding energy shift in the valence energy region in PES and IPES in terms of a "total energy" approach in Section 4.2 and the assignments in PES and SRPES in terms of a "molecular orbital" picture in Section 4.3. Finally, in Section 4.4 we deal with the preliminary results of core and Auger spectra and consider the extra-atomic relaxation of these spectra by means of the method used in Section 4.2.

4.2. Binding energy shift in photoelectron spectroscopy and inverse photoelectron spectroscopy

We shall consider the binding energy or ionization energy shift observed in PES as well as IPES from the point of view of a total energy approach. We shall first consider the binding energy shifts observed in the 5p level. The binding energy shift is again written as

$$-\Delta I = I^{v}_{ads} - I^{v}_{gas} \tag{10}$$

The magnitude of I^{v}_{gas} can be obtained from the values of the ionization energy I^{F}_{ads} with respect to the Fermi level, the work function ϕ of the metal and the change $\Delta\phi$ in work function of the metal as a result of adsorption. Therefore I^{v}_{ads} can be written as

$$I^{v}_{ads} = I^{F}_{ads} + \phi - \Delta\phi \tag{11}$$

Ionization energies are defined as

$$I^{v}_{gas} = E(Xe^{+}) - E(Xe) \tag{12}$$

$$I^{v}_{ads} = E(MXe^{+}) - E(MXe) \tag{13}$$

where the E refers to the total energies of the systems of xenon, Xe^{+} etc. as indicated in the parentheses.

The interaction energies of the systems can also be similarly defined by

$$-\Delta E = E(MXe) - \{E(M) + E(Xe)\} \tag{14}$$

$$-\Delta E^{+} = E(MXe^{+}) - \{E(M) + E(Xe^{+})\} \tag{15}$$

where the hole after ejection of an electron is assumed to be located in the xenon atom. Schematic potential energy curves of the MXe^{+} and MXe systems are shown in Fig. 7. Substituting $-\Delta E^{+}$ from $-\Delta E$ and using eqns. (10), (12) and (13), one obtains

$$\Delta E^{+} - \Delta E = I^{v}_{gas} - I^{v}_{ads} = \Delta I \tag{16}$$

It is clear that ΔI can be represented in terms of ΔE and ΔE^{+}. Therefore one can rationally write two quantities ΔI_i and ΔI_f and the corresponding magnitudes of

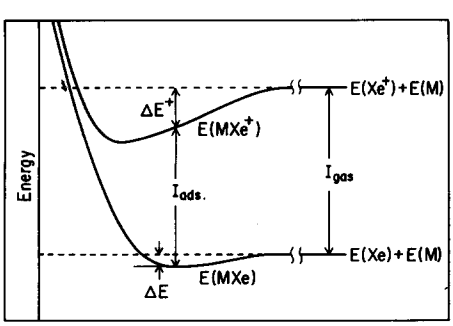

Fig. 7. Schematic potential energy curves for xenon and its ion adsorbed on metal surfaces.

these parameters for the initial and final state effects as follows:

$$\Delta I_i = -\Delta E; \Delta I_f = \Delta E^+ \tag{17}$$

From a comparison between the magnitudes of ΔE^+ and ΔE for (A) in Table VI we can obtain the inequality $\Delta E^+ \gg \Delta E$, which shows that the shift in binding energy is mainly due to the final state effect[111,112].

If one were interested in the binding energy shift as a function of the number of layers, one could define the ionization energy values in terms of the various adsorbed layers formed on the surface. For example, for the first two layers, one can write the following equations:

$$I^v_{ads}(1) = I^v_{ads} + \phi - \Delta\phi(1) \tag{18}$$

$$I^v_{ads}(2) = I^v_{ads} + \phi - \Delta\phi(2) \tag{19}$$

Here (1) refers to adsorption on the bare metal surface and (2) refers to adsorption on the first layer. Then one can define the binding energy shift as a result of the formation of the second layer with respect to that of the first layer as follows:

$$\begin{aligned}\Delta I(1\text{–}2) &= I^v_{ads}(2) - I^v_{gas}(1) \\ &= \{I^F_{ads}(2) - I^F_{gas}(1)\} - \{\Delta\phi(2) - \Delta\phi(1)\} \\ &= \Delta I^F_{ads} - \Delta(\Delta\phi)\end{aligned} \tag{20}$$

On the contrary, the binding energy shift of the first two layers can also be written in terms of the equations

$$I^v_{gas} - I^v_{ads}(1) = \Delta I(1) = \Delta E^+(1) - \Delta E(1) \tag{21}$$

$$I^v_{gas} - I^v_{ads}(2) = \Delta I(2) = \Delta E^+(2) - \Delta E(2) \tag{22}$$

So, from eqns. (21) and (22), one can deduce the change in binding energy on going from the first layer to the second layer as follows:

$$\begin{aligned}\Delta I(1\text{–}2) &= \{\Delta E^+(1) - \Delta E^+(2)\} - \{\Delta E(1) - \Delta E(2)\} \\ &= \Delta(\Delta E^+) - \Delta(\Delta E)\end{aligned} \tag{23}$$

Therefore, from eqns. (20) and (23) one obtains

$$\Delta I^F_{ads} - \Delta(\Delta\phi) = \Delta(\Delta E^+) - \Delta(\Delta E) \tag{24}$$

It is clear that one can obtain the value of $\Delta(\Delta E^+)$ since $\Delta I^F_{ads}(j)$, $\Delta\phi(j)$ and $\Delta E(j)$ ($j = 1,2$) are experimentally observable quantities. The values of $\Delta(\Delta E^+)$ deduced by using eqn. (24) as well as experimental data for a typical set of chosen systems are given in Table VII.

In the case of xenon adsorption on Pd(100)[18] as well as Ag(111)[21], there is a considerable work function change on adsorption while little or no work function change is observed for xenon adsorption on polycrystalline caesium surfaces[107] as well as Pb/Ni(111)7×7 [114] systems, probably because these two may correspond to very weak adsorption systems.

We shall consider the quantities given in Table VII. The binding energy values

$I^{F}_{ads}(1)$ and $I^{F}_{ads}(2)$ are the experimentally observable quantities. The change $\Delta\phi(1)$ in work function as a result of adsorption on the bare systems is also experimentally observable. $\Delta\phi(2)$, the corresponding quantity for the second layer, is not easily observed, but it has been reported for Ag(111). However, one can assume that $\Delta\phi(2)$ will be similar in magnitude to $\Delta\phi(1)$. Therefore, $\omega(\Delta\phi) = \Delta\phi(2) - \Delta\phi(1) = 0$. $\Delta E(1)$ and $\Delta E(2)$, the interaction energies resulting from adsorption, are also observable from desorption spectra. For Cs(poly) as well as Pb/Ni(111)7×7, $\Delta E(2)$ is not experimentally determined, but one can propose that $\Delta E(2)$ will be of similar magnitude to $\Delta E(1)$. Therefore $\Delta(\Delta E)$ will be almost equal to zero.

It is seen from the values for $\Delta(\Delta E^{+})$ given in Table VII that its magnitude is greater than that of $\Delta(\Delta E)$ except for Cs(poly). This situation shows that the observed binding energy shift should therefore be associated more with the final state effect than the initial state effect.

We shall consider the treatment of Jacobi[114] in relation to the approach presented above. Jacobi used two terms, "ΔE_R" and "$\Delta\phi$", to denote the final and initial state effects respectively. It should be remembered that the binding energy shift considered by Jacobi is denoted by I^{F}_{ads}, which is different from that denoted in the present approach by $\Delta I(1\text{–}2)$. The equivalents of the expressions derived here in terms of Jacobi's notation are

$$I^{F}(j) \rightarrow E^{F}_{B}(j) \quad (j = 1,2)$$

$$\Delta E^{+}(j) \rightarrow E_{R}(j)$$

It is clear that Jacobi's expressions are also obtainable from the present approach. Thus if $\Delta(\Delta E)$ is neglected in eqn. (24), one obtains

$$\Delta E^{F}_{B} = \Delta(\Delta\phi) + E_{R} \tag{25}$$

Assuming $\Delta(\Delta\phi) = 0$ in eqn. (25), Jacobi obtains

$$\Delta E^{F}_{B} = \Delta E_{R} \tag{26}$$

This is the expression corresponding to the final state model (ΔE_R). In the case of the initial state effect model ($\Delta\phi$), $E_R(j) = 0$, so that Jacobi obtains

$$\Delta E_{R} = \Delta(\Delta\phi) \tag{27}$$

Jacobi showed that the result of eqn. (27) is inconsistent with that observed for the Xe–Pb/Ni(111)7×7[114] system ($\Delta E^{F}_{B} = 0.5$ eV, $\Delta\phi = 0$; see Table VII), so that the observed binding energy shifts could be mostly due to a final state effect.

Jacobi has used two independent relations (26) and (27) to deduce whether the binding energy shift is due to an initial state effect or a final state effect. The present approach considers both of the effects in the form of a single equation and the relative magnitudes of the terms are used to decide which effect is responsible for the observed binding energy shift.

Finally, we shall discuss the 6s binding energy shifts obtained in IPES[115,116]. The 6s level is unoccupied in the ground state of the adsorption system. The final state in IPES is a negative ion state. Since IPES is the inverse of the PES process, one can write down equations for the IPES process in a similar manner to that for PES

TABLE VII

OBSERVED VALUES OF Xe $5p_{1/2}$ PEAK POSITIONS WITH RESPECT TO THE FERMI LEVEL I^F, WORK FUNCTION CHANGES $\Delta\phi$ (i) AND DESORPTION ENERGIES $\Delta E(i)$ $(i = 1,2)$ OF EACH LAYER ON A VARIETY OF METAL SURFACES

Substrate	$I^F_{ads}(1)$ (eV)	$I^F_{ads}(2)$ (eV)	ΔI^F_{ads} (eV)	$\Delta\phi(1)$ (eV)	$\Delta\phi(2)$ (eV)	$\Delta(\Delta\phi)$ (eV)	$\Delta E(1)$ (eV)	$\Delta E(2)$ (eV)	$\Delta(\Delta E)$ (eV)	$\Delta(\Delta E^+)$[a] (eV)	*Reference*
Pd(100)	6.95	7.60	0.65	0.86		0[b]	0.35	0.22	0.13	0.78	18
Ag(111)	7.62	8.15	0.53	0.47	<0.6	<-0.13	0.23	0.17	0.06	0.46	21
Cs(poly)	10.6	10.6	0	≈ 0		0[b]	0.13[c]		0[b]	0	107
Pb/Ni(111)7 × 7	7.0	7.5	0.5	0.05		0[b]	≈ 0.17[b]		0[b]	0.5	114

[a] Values of $\Delta(\Delta E^+)$ calculated with eqn. (24).

[b] Values are indicated implicitly from the experimental studies.

[c] Value estimated from the maximum desorption temperature (50 K) by the use of Redhead's equation for first-order desorption with $\nu = 10^{13}\ s^{-1}$.

TABLE VIII

OBSERVED VALUES OF 6s PEAK POSITIONS WITH RESPECT TO THE FERMI LEVEL I^F, WORK FUNCTION CHANGES $\Delta\phi$ (i) AND ADSORPTION ENERGIES $\Delta E(i)$ $(i = 1,2)$

Substrate	$I^F_{ads}(1)$ (eV)	$I^F_{ads}(2)$ (eV)	ΔI^F_{ads} (eV)	$\Delta\phi(1)$ (eV)	$\Delta\phi(2)$ (eV	$\Delta(\Delta\phi)$ (eV)	$\Delta E(1)$ (eV)	$\Delta E(2)$ (eV)	$\Delta(\Delta E)$ (eV)	$\Delta(\Delta E^-)$[a] (eV)	*Reference*
Au(poly)	3.00	3.65	0.65	0.45	0	0	0.23	0.17	0.06	0.71	115
Ru(0001)	4.50	3.30	−1.20	0.80	0	0	0.35	0.22	0.13	−1.07	116

[a] Calculated with eqn. (24a).

but using electron affinity $I^v = E(A^-) - E(A)$ instead of ionization energy in eqns. (12) and (13) as well as using the species E^- instead of E^+ in the equation:

$$\Delta I^F_{ads} - \Delta(\Delta\phi) = \Delta(\Delta E^-) - \Delta(\Delta E) \tag{24a}$$

6s binding energy data are given in Table VIII. From the values it is clear that the magnitude of $\Delta(\Delta E^-)$ is larger than the magnitude of $\Delta(\Delta E)$. This shows that the shift in binding energy is due to the final state effect even for the IPES process.

It should be noted that the signs of the $\Delta(\Delta E^-)$ values are opposite for the two systems considered in Table VIII. The negative value implies that the interaction in subsequent higher layers is greater than that for the first layer with the metal surface. This appears to be implicitly incorrect. This fallacy could have arisen from some problem in the case of results reported by Wandelt *et al.* for the multilayer adsorption of xenon on Ru(0001) [116].

4.3. Assignment in photoelectron spectroscopy and spin-resolved photoelectron spectroscopy

4.3.1. Splitting mechanism of the μ_1 peak

In this section we discuss the mechanism of the splitting of peaks observed in UPS spectra for xenon adsorbed on metals. Typical spectra obtained are shown in Fig. 4. Hereafter we focus on the μ_1 peak.

When xenon atoms approach metal surfaces it is expected that degenerate 5p orbitals can be resolved owing to interaction with the metal surfaces. The electronic configuration of the ground state of a free xenon atom is $\ldots(5p)^6$; the 5p orbitals of xenon on adsorption give rise to two states designated as $5p\sigma$ and $5p\pi$. In this description one assumes that the metal possesses a large number of electrons with suitable energy and symmetry for molecular orbital formation and the metal levels in the ground state are filled up to the Fermi level. Therefore the electronic configuration of adsorbed xenon is given by $\ldots(5p\sigma)^2(5p\pi)^4$. In the spectroscopic notation for linear molecules this corresponds to a $^1\Sigma$ state[5]. The two mono-ionic states possible for xenon have the configurations $(5p\sigma)^1(5p\pi)^4$ with a $^2\Sigma$ state and $(5p\sigma)^2(5p\pi)^3$ with a $^2\Pi$ state. The level $^2\Pi$ can be further split owing to SO interaction into two degenerate states $^2\Pi_{1/2}$ and $^2\Pi_{3/2}$. In Fig. 8 schematic diagrams of the orbital picture for the two states $^2\Sigma$ and $^2\Pi$ are shown. From the total energy point of view the ordering of energy levels between two states will be $E(^2\Sigma) < E(^2\Pi)$. The ionic ground state for the xenon molecule (Xe_2) should therefore be $^2\Sigma_{1/2}$ which

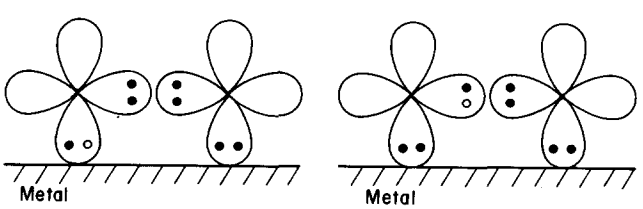

(a) (b)

Fig. 8. Schematic representation of interaction between orbitals of Xe^+ and metal surfaces in (a) $^2\Sigma$ and (b) $^2\Pi$ states: ●, occupied electron; ○, hole.

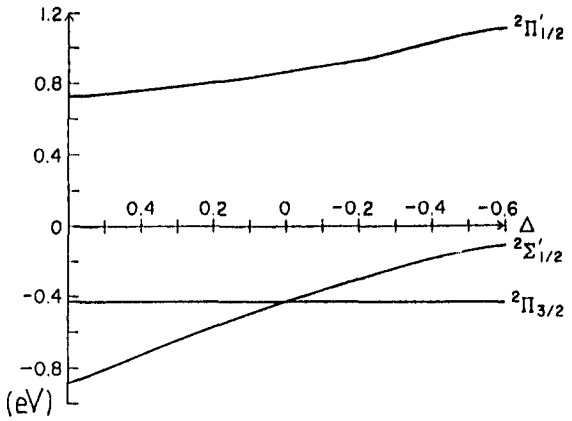

Fig. 9. Calculated position of energy levels as a function of the parameter Δ.

has also been confirmed experimentally and theoretically[5]. This situation may hold good for the adsorption system (see Fig. 9).

Energy level ordering of various ionic states can be determined by the use of the variation method. The total wavefunction of the system can be written as

$$\Psi = \sum_{i=1}^{3} a_i \varphi_i \tag{28}$$

The secular equation is

$$| H_{ij} - \delta_{ij} E | = 0 \tag{29}$$

where δ_{ij} is Kronecker's delta and H_{ij} is defined as

$$H_{ij} = \langle \varphi_j | H_0 + H' | \varphi_i \rangle = E_i \delta_{ij} + H'_{ij} \tag{30}$$

where H_0 is the total spinless electronic hamiltonian and H' is the hamiltonian corresponding to SO interaction, the effect of which is approximated by the use of the empirical method. The diagonal elements H_{ij} are E_1, $E_2 + \xi/2$ and $E_3 - \xi/2$ where ξ is the SO parameter, which is taken to be 0.87 eV for the free xenon ion[4], and $E_2 = E_3$. The off-diagonal elements are given by

$$\langle \varphi(^2\Sigma_{1/2}) | H' | \varphi(^2\Pi_{1/2}) \rangle = 2\xi/2 = 2\eta \tag{31}$$

and its conjugate term since the states with the same total angular momentum interact with each other and $\xi/2 = \eta$. The determinant form of the secular equation is explicitly given by

$$\begin{vmatrix} E_1 - E & 2\eta & 0 \\ 2\eta & E_2 + \eta - E & 0 \\ 0 & 0 & E_3 - \eta - E \end{vmatrix} = 0 \tag{32}$$

One can obtain the energy level positions of the states as a function of the parameter defined as $\Delta = E_2 - E_1 = E(^2\Pi) - E(^2\Sigma)$ (Fig. 9). When $\Delta = 0$, the splitting would correspond to that observed for gaseous xenon, namely 1.3 eV.

When $\Delta = 0.4\,\text{eV}$, the wavefunctions can be written as linear combinations as follows:

$$\varphi(^2\Sigma'_{1/2}) = a_1\varphi(^2\Sigma_{1/2}) + a_2\varphi(^2\Pi_{1/2}) \tag{33a}$$

$$\varphi(^2\Pi'_{1/2}) = b_1\varphi(^2\Sigma_{1/2}) + b_2\varphi(^2\Pi_{1/2}) \tag{33b}$$

The coefficients satisfy the identities $a_1^2 = b_2^2 = 0.78$ and $b_1^2 = a_2^2 = 0.22$ when $\Delta = 0.4\,\text{eV}$. When $\Delta = 0$, the coefficients satisfy the following identities: $a_1^2 = b_2^2 = 2/3, b_1^2 = a_2^2 = 1/3$. The latter set of values of the coefficients correspond to that of gaseous xenon. Therefore the changes in the values of the coefficients of the former set appear to be due to a bonding effect in adsorption. At more negative values of Δ, the energy level positions will alter such that the resultant ordering would be $E(^2\Sigma) > E(^2\Pi)$. In this case the ground state would be $^2\Pi_{3/2}$. However, this situation seems to be unrealistic, at least at low coverages. In fact, the observations as a function of coverage by Opila and Gomer[94] as well as by Onellion and Erskine[117] reveal the splitting even at low coverages. To resolve the controversy in the assignment one needs measurements with SRPES at very low coverages without lateral Xe–Xe interaction.

4.3.2. Assignment of excitation spectra

The SRPES spectra for excited states have been reported[23]. These results for xenon adsorbed on graphite are shown in Fig. 5. It is seen that there are four peaks in the energy range 8–10 eV. The exact positions of the peaks observed are at 8.1, 8.45, 9.05, and 9.50 eV. For convenience we number them 1, 2, 3, and 4. It is seen that the intensity of peak 3 is small compared with those of the other three peaks. The separation between peaks 1 and 2 is 0.35 eV, while that between peaks 2 and 3 is 0.60 eV and that between peaks 3 and 4 is 0.45 eV. The corresponding separations of the gaseous xenon spectrum are 0.12 eV, 1.01 eV and 0.12 eV respectively. The total separation is 1.25 eV for gaseous xenon[4] while it is 1.44 eV in the case of adsorbed xenon. The reason for this broadening could be the interaction of excited xenon with metal surfaces.

Let us consider the assignment of the four peaks in Fig. 5(b). For the adsorption of excited state xenon atoms various multiplet states are possible. The electronic configuration of the neutral ground state of adsorbed xenon is $\ldots(5p\sigma)^2(5p\pi)^4$. The configurations of the next immediate excited states are obtained by promotion of a $5p\sigma$ or $5p\pi$ electron into the $6s\sigma$ level. Then electronic configurations and term symbols are $(5p\sigma)^1(5p\pi)^4(6s\sigma)^1$, $^3\Sigma$, $^1\Sigma$, and $(5p\sigma)^2(5p\pi)^3(6s\sigma)^1$, $^3\Pi$, $^1\Pi$, respectively. The triplet $^3\Sigma$ states will give rise to $^3\Sigma_1$, $^3\Sigma_0$ multiplets while the $^3\Pi$ state will give rise to $^3\Pi_2$, $^3\Pi_1$, $^3\Pi_{0+}$, $^3\Pi_{0-}$ states. A total of eight multiplet states are possible for these two excited state configurations. Thus the total wavefunction Ψ can be written as

$$\Psi = \sum_{i=1}^{8} a_i\varphi_i$$

The multiplet energy levels can be calculated in a similar way to the assignment of PES peaks. For more details concerning this, the reader is referred to ref. 118.

Finally, a brief comment on the original interpretation of Cunningham *et al.*[119] is in order. They observed a peak at an energy of 8 eV for xenon adsorption on

magnesium while such a peak was absent for the case of xenon adsorbed on gold. They discussed this observation in terms of an optical switch model which considers the relative positions of the highest occupied level of xenon and that of the metal as well as the magnitudes of the work function values for the two metals under discussion. This interpretation led to a number of theoretical studies (see for example ref. 120). However, Demuth *et al.*[93] reported the EELS spectra for the system of xenon adsorbed on gold. They could observe the peak around 8 eV even at low coverages. It is therefore clear that there seems to be still some controversy[93,121] regarding the observation of excited state spectra of adsorbed xenon.

4.4. Core and Auger spectra

Core electron ejection is possible only with a high energy incident beam. Yates and Erickson[122] used the intensity of the X-ray photoelectron spectroscopy $3d_{5/2}$ peak for the estimation of the quantities of xenon adsorbed. Kaindl *et al.*[72,110] examined the shapes of $4d_{5/2}$ and $4d_{3/2}$ emissions and could even deduce from the peak shapes the extent of coverage in terms of number of layers adsorbed.

In Fig. 10[110], 4d core spectra of xenon adsorbed on Pd(100) as well as 5p valence spectra are shown for a synchroton radiation source and an incident energy of 90 eV. The line spectra a, b and c correspond to respectively 1, 2 and 4 layer adsorption. The binding energy values given are with respect to the vacuum level. In spectra b and c, the dotted resolved peaks are due to the first layer while the peaks with broken lines are due to multilayers above the first layer. First layer formation could be distinguished from that of subsequent multilayers because of the high resolution facility available in the equipment. The separation between the monolayer peak and the peak due to the second layer as shown in Fig. 10 is 0.72 eV and the

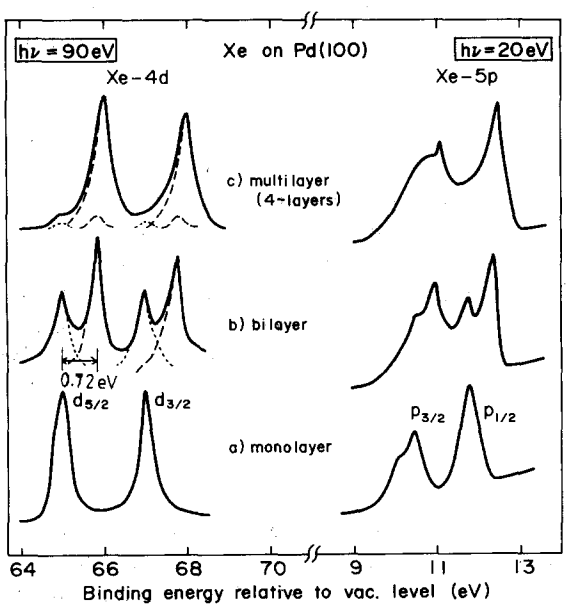

Fig. 10. 4d core and 5p valence spectra for Xe–Pd(100)[72,110].

subsequent layer peaks shift to higher binding energy values, thus tending to those of the gas species, namely 67.5 eV for $4d_{5/2}$ and 69.5 eV for $4d_{3/2}$ (ref. 4).

In Fig. 11[110], NOO Auger spectra of xenon adsorbed on Pd(100) are shown. The arrow in spectrum a corresponds to the $N_5O_{2,3}O_{2,3}$ transition. In spectra b and c, the contributions to the Auger transition from the first layer (dotted line), from the second layer (broken line) and from subsequent layers (chain line) are shown. In Table IX the available data for the shift in the 4d level as well as Auger transitions are given as a function of the extent of adsorption in terms of number of layers. It is seen that the shifts in the core level binding energy as well as the shift in the Auger transition are higher for the first layer while the shifts for subsequent layers are relatively small. The magnitude of this shift in the Auger transition is almost three times the shift observed in the core level binding energy. This difference could be

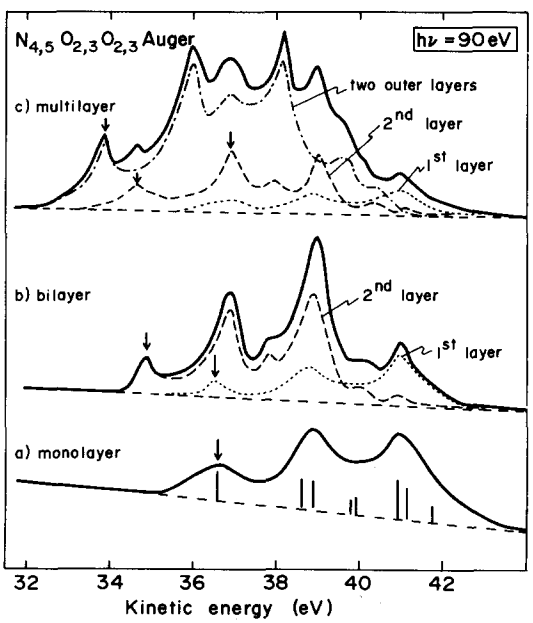

Fig. 11. NOO Auger spectra as a function of number of layers for Xe–Pd(100) [72,110].

TABLE IX

4d BINDING ENERGY SHIFTS AND NOO AUGER SHIFTS WITH RESPECT TO FREE ATOMS FOR XENON OVERLAYERS ON Pd(100) [72,110]

Xe configuration	*Layer*	$\Delta I(4d)$ (eV)	$\Delta(Auger)$ (eV)	$\Delta(Auger)/\Delta I(4d)$
Monolayer	1st	2.14	6.57	3.07
Bilayer	1st	2.21	6.70	3.13
	2nd	1.49	4.69	3.15
Multilayer	1st	2.24	6.79	3.03
	2nd	1.54	4.75	3.08
	Outer	1.28	4.89	3.82

rationalized in terms of the final state effect since in the Auger transition the final state corresponds to the doubly positively charged ion, while in the core level spectra the final state is only a singly charged ion. Following the discussion reported by Mullins *et al.*[62], we shall evaluate this difference between the final state effects by use of the Auger parameter A_* for an adsorbed atom, which is written

$$A_* = E^{\text{out}}_*(\text{AES}) - E^{\text{out}}_*(\text{PES}) \tag{34}$$

where * indicates the adsorbed (ads) or gaseous (gas) system, and $E^{\text{out}}_*(\text{AES})$ and $E^{\text{out}}_*(\text{PES})$ are the kinetic energies of an Auger and a core photoelectron respectively.

The $E^{\text{out}}_*(\text{AES})$ are given in terms of energy conservation and the notation used in Section 4.2:

$$E^{\text{out}}_{\text{ads}} = E^{\text{in}} - I^{\text{v}}_{\text{ads}}(\text{AES}), \quad I^{\text{v}}_{\text{ads}}(\text{AES}) = E(\text{MXe}^{2+}) - E(\text{MXe}) \tag{35}$$

$$E^{\text{out}}_{\text{gas}} = E^{\text{in}} - I^{\text{v}}_{\text{gas}}(\text{AES}), \quad I^{\text{v}}_{\text{gas}}(\text{AES}) = E(\text{Xe}^{2+}) - E(\text{Xe}) \tag{36}$$

where $I^{\text{v}}_{\text{ads}}(\text{AES})$ represents the "apparent binding energy" in Auger spectroscopy. The notation and the explanation of $E^{\text{out}}_*(\text{PES}) = E^{\text{in}} - I^{\text{v}}_*(\text{PES})$ have already been given in Section 4.2. With these equalities, the Auger parameter (eqn. (34)) can be written in the alternative form

$$\begin{aligned} A_{\text{ads}} = E^{\text{out}}_{\text{ads}}(\text{AES}) - E^{\text{out}}_{\text{ads}}(\text{PES}) &= -\{I^{\text{v}}_{\text{ads}}(\text{AES}) - I^{\text{v}}_{\text{ads}}(\text{PES})\} \\ &= -\{E(\text{MXe}^{2+}) - E(\text{MXe}^{+})\} \end{aligned} \tag{37}$$

$$\begin{aligned} A_{\text{gas}} = E^{\text{out}}_{\text{gas}}(\text{AES}) - E^{\text{out}}_{\text{gas}}(\text{PES}) &= -\{I^{\text{v}}_{\text{gas}}(\text{AES}) - I^{\text{v}}_{\text{gas}}(\text{PES})\} \\ &= -\{E(\text{Xe}^{2+}) - E(\text{Xe}^{+})\} \end{aligned} \tag{38}$$

Subtracting eqn. (38) from eqn. (37), we have

$$\begin{aligned} A_{\text{ads}} - A_{\text{gas}} &= -[\{E(\text{MXe}^{2+}) - E(\text{Xe}^{2+})\} - \{E(\text{MXe}^{+}) - E(\text{Xe}^{+})\}] \\ &= -([E(\text{MXe}^{2+}) - \{E(\text{Xe}^{2+}) + E(\text{M})\}] - [E(\text{MXe}^{+}) \\ &\quad - \{E(\text{Xe}^{+}) + E(\text{M})\}]) \\ &= -(\Delta E^{2+} - \Delta E^{+}) \end{aligned} \tag{39}$$

where ΔE^{2+} is the interaction energy between the substrate and an ionized atom adsorbed with two holes by analogy with eqns. (13) and (14) (Section 4.2). The expression of eqn. (39) is consistent with that of eqn. (16) (Section 4.2). It is obvious from eqn. (39) that the term $A_{\text{ads}} - A_{\text{gas}}$, which will be denoted by $R(\text{surf})$, represents the difference in the final states, *i.e.* the extra-atomic relaxation, between the Auger and PES processes.

It is concluded from Section 4.2 that the binding energy ΔI is predominantly due to the final state effect ΔE^{+}; that is, $\Delta I \approx \Delta E^{+}$. A similar conclusion may be obtained in AES: $\Delta(\text{Auger}) \approx \Delta E^{2+}$. The ratios $\Delta(\text{Auger})/\Delta I(4\text{d})$ in Table IX are

$$\frac{\Delta(\text{Auger})}{\Delta I(4\text{d})} = \frac{\Delta E^{2+}}{\Delta E^{+}} \approx 3, \text{ or } \Delta E^{2+} \approx 3\,\Delta E^{+} \tag{40}$$

Substituting $3\,\Delta E^{+}$ for ΔE^{2+} in the right-hand side of eqn. (39), we have

$$R(\text{surf}) = -2\,\Delta E^{+} \approx 2\,\Delta I \tag{41}$$

Equation (41) shows that a first approximation for R(surf) proposed by Stair (ref. 123, cited in ref. 62) is proper empirically. On the contrary, if ΔE^+ and ΔE^{2+} are represented by classical image energies $e^2/4D$ and $(2e)^2/4D$ respectively, the magnitude of R(surf) is given by

$$R(\text{surf}) = -3\,\Delta E^{2+} \approx 3\,\Delta I \tag{42}$$

The difference between the coefficients 2 and 3 in eqns. (41) and (42) respectively shows that the approximation $R(\text{surf}) = 2\,\Delta I$ cannot be justified from a theoretical standpoint by the classical image method.

5. SUMMARY

Normally inert gas adsorption on metal surfaces is considered to be a weak interaction system. However, the available data on the energetics of xenon adsorption on metal surfaces and the work function changes as a result of adsorption reveal the inadequacy of treating this system in terms of simple van der Waals' forces.

Comprehensive analyses of available experimental data, especially probed through a number of surface analytical tools such as PES as well as IPES, show that a chemical bonding model may be better suited for the description of this system. The features (normally splitting) observed by PES as well as IPES for xenon adsorption on metal surfaces have been rationalized within the framework of this model. The relative importance of relaxation parameters and initial state chemical effects for the observed shifts in emission features of electron spectroscopic observations has been evaluated.

REFERENCES

1 B. E. Nieuwenhuys, *Ned. Tijdschr. Vacuumtech.*, *13* (1975) 41, and references cited therein.
2 K. Siegbahn *et al.*, *ESCA applied to Free Molecules*, North-Holland, Amsterdam, 1969.
3 D. W. Turner, G. Baker, A. D. Baker and C. R. Brundle, *Molecular Photoelectron Spectroscopy*, Interscience, London, 1970.
4 C. E. Moore, *Atomic Energy Levels, NBS Circ. 467*, 1958 (National Bureau of Standards).
5 K. P. Huber and G. Herzberg, *Constants of Diatomic Molecules*, Van Nostrand Reinhold, New York, 1979.
6 C. Kittel, *Introduction to Solid State Physics*, Wiley, New York, 4th edn., 1971.
7 T. Mandel, K. Kaindl, M. Domke, W. Fisher and N. D. Schneider, *Phys. Rev. Lett.*, *55* (1985) 1638.
8 T. Yoneda, Y. Sagisaka, M. Orichi, H. Kato, S. Suzuki, K. Izdamoto and Y. Aiura, personal communication, 1989.
9 K. Christmann and J. E. Demuth, *Surf. Sci.*, *120* (1982) 291.
10 M. A. Chesters, M. Hussain and J. Pritchard, *Surf. Sci.*, *35* (1973) 161.
11 M. A. Chesters and J. Pritchard, *Surf. Sci.*, *28* (1973) 460.
12 M. Jaubert, A. Glachant, M. Bienfait and G. Boato, *Phys. Rev. Lett.*, *46* (1981) 1679.
13 A. Glachant, M. Jaubert, M. Bienfait and G. Boato, *Surf. Sci.*, *115* (1981) 115.
14 A. Glachant, M. Jaubert, M. Bienfait and M. Jaubert, *Surf. Sci.*, *148* (1984) L665.
15 W. Berndt, *Surf. Sci.*, *219* (1989) 219.
16 R. H. Roberts and J. Pritchard, *Surf. Sci.*, *54* (1976) 687.
17 H. Papp and J. Pritchard, *Surf. Sci.*, *53* (1975) 371.
18 K. Wandelt and J. Hulse, *J. Chem. Phys.*, *80* (1984) 1340.

19 P. W. Palmberg, *Surf. Sci.*, *25* (1971) 598.
20 G. McElhiney, H. Papp and J. Pritchard, *Surf. Sci.*, *54* (1976) 617.
21 R. J. Behm, C. R. Brundle and K. Wandelt, *J. Chem. Phys.*, *85* (1986) 1061.
22 T. Engel, P. Bornemann and E. Bauer, *Surf. Sci.*, *81* (1979) 252.
23 G. Schönhense, *Appl. Phys. A*, *41* (1986) 39, and references cited therein.
24 A. Ignatiev, A. V. Jones and T. N. Rhodin, *Surf. Sci.*, *30* (1972) 573.
25 K. Kern, R. David, P. Zeppenfeld and G. Comsa, *Surf. Sci.*, *195* (1988) 353.
26 A. Cassuto, J. J. Ehrhardt, J. Cousty and R. Riwan, *Surf. Sci.*, *194* (1988) 453.
27 P. Bak, D. Mukamel, J. Villain and K. Wentowska, *Phys. Rev. B*, *19* (1979) 1610.
28 V. L. Pokrovsky and A. L. Talapov, *Phys. Rev. Lett.*, *42* (1979) 65.
29 A. Glachant and U. Bardi, *Surf. Sci.*, *87* (1979) 187.
30 P. Dolle, M. Alnot, J. J. Ehrhardt, A. Thomy and A. Cassuto, *C.R. Acad. Sci. II*, *296* (1983) 529.
31 R. Miranda, S. Daiser, K. Wandelt and G. Ertl, *Surf. Sci.*, *131* (1983) 61.
32 R. Opila and R. Gomer, *Surf. Sci.*, *112* (1981) 1.
33 J. C. P. Mignolet, *Discuss. Faraday Soc.*, *8* (1950) 105.
34 J. C. P. Mignolet, *J. Chem. Phys.*, *21* (1953) 1298.
35 H. Margenau and N. R. Kestner, *Theory of Intermolecular Forces*, Pergamon, Oxford, 2nd edn., 1971, Chap. 9.
N. H. March, *Chemical Bonds Outside Metal Surfaces*, Plenum, New York, 1986.
36 W. E. Garner (ed.), *Chemisorption*, Butterworths, London, 1957, p. 118.
37 R. Mulliken, *J. Am. Chem. Soc.*, *74* (1952) 811.
F. A. Matsen, A. C. Makrides and N. Hackerman, *J. Chem. Phys.*, *22* (1954) 1800.
38 P. M. Gundry and F. C. Tompkins, *Trans. Faraday Soc.*, *56* (1960) 846.
39 T. Engel and R. Gomer, *J. Chem. Phys.*, *52* (1970) 5572.
40 B. E. Nieuwenhuys, O. G. van Aardenne and W. M. H. Sachtler, *Chem. Phys.*, *5* (1974) 418.
41 C. P. Flynn and Y. C. Chen, *Phys. Rev. Lett.*, *46* (1981) 447.
42 S. Ishi, *Shokubai*, *20* (1978) 191; *Hyomen*, *10* (1989) 340 (in Japanese).
43 G. Oxinos and A. Modinos, *Surf. Sci.*, *89* (1979) 292.
44 N. D. Lang, *Phys. Rev. Lett.*, *46* (1981) 824.
45 R. A. Kromhout and B. Linder, *J. Chem. Phys.*, *81* (1984) 2516.
46 K. Wandelt and B. Gumhalter, *Surf. Sci.*, *140* (1984) 355.
47 R. Suhrmann, E. A. Dierck, B. Engelke, H. Hermann and K. Schulz, *Naturwissenschaften*, *43* (1956) 127; *J. Chim. Phys.*, *54* (1957) 15.
48 G. Ehrlich and F. G. Hudda, *J. Chem. Phys.*, *30* (1959) 493.
49 R. Gomer, *J. Chem. Phys.*, *29* (1958) 441.
50 W. J. M. Rootsaert, L. L. van Reijen and W. M. H. Sachtler, *J. Catal.*, *1* (1962) 416.
51 K. Ishizuka, *J. Res. Inst. Catal. Hokkaido Univ.*, *15* (1967) 95.
52 B. E. Nieuwenhuys and W. M. H. Schatler, *Surf. Sci.*, *45* (1974) 513.
53 B. E. Nieuwenhuys, D. Th. Meijer and W. M. H. Schatler, *Phys. Status Solidi A*, *24* (1974) 115.
54 H. H. Rotermund and K. Jacobi, *Solid State Commun.*, *44* (1982) 483.
K. Jacobi, Y.-p. Hsu and H. H. Rotermund, *Surf. Sci.*, *114* (1982) 683.
55 K. C. Prince, C. Klauber and B. G. Baker, *Proc. IVC-8, ICSS-4, ECOSS-3, Cannes*, in *Vide, Couches Minces, Suppl.*, *III* (1980) 1170.
56 Y. C. Chen, J. E. Cunningham and C. P. Flynn, *Phys. Rev. B*, *30* (1984) 7317.
57 D. F. Klemperer and J. C. Snaith, *Surf. Sci.*, *28* (1971) 209; *45* (1974) 318.
58 T.-C. Chiang, G. Kaindl and D. E. Eastman, *Solid State Commun.*, *36* (1980) 25.
59 J. Müller, *Ber. Busenges. Phys. Chem.*, *79* (1975) 123; *Surf. Sci.*, *42* (1974) 525; *45* (1974) 314.
60 M. Mohri, *Ph.D. Thesis*, Flinders University of South Australia, 1975.
61 D. Menzel, in M. Grunze and H. J. Kreuzer (eds.), *Kinetics of Interface Reactions*, Springer Series on Surface Science, Springer, Berlin, 1986, p. 2.
62 D. R. Mullins, J. M. White and H. S. Luftman, *Surf. Sci.*, *167* (1986) 39.
63 K. Jacobi and H. H. Rotermund, *Surf. Sci.*, *116* (1982) 435.
64 C. Mariani, K. Horn and A. M. Bradshaw, *Phys. Rev. B*, *25* (1982) 7798.
65 U. Bardi, A. Glachant and M. Bienfait, *Surf. Sci.*, *97* (1980) 137.
66 N. Hansen and W. Littmann, *Ber. Bunsenges. J. Phys. Chem.*, *67* (1963) 970.

67 G. Ehrlich, *Br. J. Appl. Phys.*, *15* (1964) 349.
68 K. Wandelt, J. Hulse and J. Kuppers. *Surf. Sci.*, *104* (1981) 212.
69 I. T. Steinberger and K. Wandelt, *Phys. Rev. Lett.*, *58* (1987) 2494.
70 B. E. Nieuwenhuys, R. Bouwman and W. M. H. Schatler, *Thin Solid Films*, *21* (1974) 51.
71 G. Erhlich, H. Heyne and C. F. Kirk, in G. A. Somorjai (ed.), *The Structure and Chemistry of Solid State Surfaces*, Wiley, New York, 1969, no. 49.
72 G. Kaindl, T.-C. Chiang, D. E. Eastman and F. J. Himpsel, in S. K. Sinha (ed.), *Ordering in Two Dimensions*, North-Holland, New York, 1980, p. 99.
73 J. Unguris, L. W. Bruch, E. R. Moog and M. B. Webb, *Surf. Sci.*, *109* (1981) 522.
74 R. F. Steiger, J. M. Morabito, Jr., G. A. Somorjai and R. H. Muller, *Surf. Sci.*, *14* (1969) 279.
75 A. G. Knapp and M. H. B. Stiddard, *J. Chem. Soc., Faraday Trans. I*, *68* (1972) 2139.
76 S. Raaen, M. Ruckman and M. Strongin, *Phys. Rev. B*, *31* (1985) 623.
77 C. Wang and R. Gomer, *Surf. Sci.*, *91* (1980) 533.
78 J. Niklibolk and Z. Dworecki, *Acta Phys. Pol.*, *32* (1967) 1023.
79 M. J. Dresser, T. E. Madey and J. T. Yates, *Surf. Sci.*, *42* (1974) 533.
80 B. Poelsema, L. K. Verheij and G. Comsa, *Surf. Sci.*, *152–153* (1985) 851.
81 G. McElhiney and J. Pritchard, *Surf. Sci.*, *60* (1976) 397.
82 J. Pritchard, *Nature (London)*, *194* (1962) 38.
83 N. D. Lang, A. R. Williams, F. J. Himpsel, B. Reihl and D. E. Eastman, *Phys. Rev. Lett. B*, *26* (1982) 1728.
84 T.-C. Chiang, G. Kaindl and D. E. Eastman, *Solid State Commun.*, *41* (1982) 661.
85 J. L. Cadrew and R. A. Pieritti, *J. Colloid Interface Sci.*, *47* (1974) 379.
86 K. Horn, C. Mariani and L. Cramer, *Surf. Sci.*, *117* (1982) 376.
87 E. R. Moog and W. B. Webb, *Surf. Sci.*, *148* (1984) 338.
88 H. Chon, R. A. Fisher, R. D. McCammon and J. G. Aston, *J. Chem. Phys.*, *36* (1962) 1378.
89 E. W. Plummer and W. Eberhardt, *Adv. Chem. Phys.*, *49* (1982) 533.
90 W. F. Egelhoff, Jr., *Surf. Sci. Rep.*, *6* (1987) 253.
91 F. J. Himpsel, *Comments Condens. Matter. Phys.*, *12* (1986) 199.
92 V. Dose, *Surf. Sci. Rep.*, *5* (1985) 339.
93 Ph. Avouris and J. E. Demuth, *Surf. Sci.*, *158* (1985) 21.
J. E. Demuth, Ph. Avouris and D. Schmeisser, *Phys. Rev. Lett.*, *50* (1983) 600.
94 R. Opila and R. Gomer, *Surf. Sci.*, *127* (1983) 569.
95 K. Wandelt, in P. Wissmann (ed.), *Chemisorption on Metal Films*, Elsevier, 1986, Chap. 7, p. 280.
96 J. E. Demuth and A. J. Schnell-Sorokin, *J. Vac. Sci. Technol. A*, *2* (2) (1984) 808.
97 B. J. Waclawski and J. F. Herbst, *Phys. Rev. Lett.*, *35* (1975) 1594.
J. F. Herbst, *Phys. Rev. B*, *15* (1977) 3720.
98 R. P. Antoniewiez, *Phys. Rev. Lett.*, *38* (1977) 374.
99 J. L. Erskine, *Phys. Rev. B*, *24* (1981) 2236.
100 J. A. D. Matthew and M. G. Devey, *J. Phys. C*, *9* (1976) L413.
101 K. Horn, M. Scheffler and A. M. Bradshaw, *Phys. Rev. Lett.*, *41* (1978) 822.
M. Scheffler, K. Horn, A. M. Bradshaw and K. Kambe, *Surf. Sci.*, *80* (1979) 69.
102 K. Hermann, J. Noffke and K. Horn, *Phys. Rev. B*, *22* (1980) 1022.
103 K. Kambe, *Surf. Sci.*, *105* (1981) 95.
104 S. Ishi and Y. Ohno, *J. Electron Spectrosc. Relat. Phenom.*, *33* (1984) 85.
105 S. Deiser and K. Wandelt, *Surf. Sci.*, *128* (1983) L213.
106 T.-C. Chiang, G. Kaindl and T. Mandel, *Phys. Rev. B*, *33* (1986) 695.
107 H. H. Rotermund and K. Jacobi, *Surf. Sci.*, *126* (1983) 32.
108 A. Gutmann, G. Zwicker, D. Schmeisser and K. Jacobi, *Surf. Sci.*, *137* (1984) 211.
109 K. Wandelt, *J. Vac. Sci. Technol. A*, *2* (1984) 802.
110 G. Kaindl, T.-C. Chiang, D. E. Eastman and F. J. Himpsel, *Phys. Rev. Lett.*, *45* (1980) 1808.
111 S. Ishi and Y. Ohno, *Surf. Sci.*, *159* (1985) L401.
112 G. Wertheim, *Appl. Phys. A*, *41* (1986) 75.
113 K. Jacobi, *Surf. Sci.*, *192* (1987) 499.
C. Astaldi and K. Jacobi, *Surf. Sci.*, *200* (1988) 15.
114 K. Jacobi, *Phys. Rev. B*, *38* (1988) 5869, 6291.

115 K. Horn, K. H. Frank, J. A. Wilder and B. Reihl, *Phys. Rev. Lett.*, *57* (1986) 1064.
116 K. Wandelt, W. Jacob, N. Memmel and V. Dose, *Phys. Rev. Lett.*, *57* (1986) 1643.
117 M. Onellion and J. L. Erskine, *Phys. Rev. B*, *33* (1987) 1440.
118 S. Ishi, H. Tatewaki and Y. Ohno, *Surf. Sci.*, *179* (1987) L13.
119 J. A. Cunningham, D. K. Greenlaw and C. P. Flynn, *Phys. Rev. B*, *22* (1980) 717.
120 C. Mavroyannis, *Mol. Phys.*, *64* (1988) 457.
121 J. Colbert, A. Zangwill and M. Strongin, *Phys. Rev. B*, *27* (1983) 1378.
122 J. T. Yates, Jr., and N. E. Erickson, *Surf. Sci.*, *44* (1974) 489.
123 P. C. Stair, *Isr. J. Chem.*, *22* (1982) 380.